

KINETICS OF GASEOUS IODINE UPTAKE ONTO STAINLESS STEEL DURING IODINE-ASSISTED CORROSION

JUNGSOOK CLARA WREN* and GLENN A. GLOWA
Atomic Energy of Canada Limited, Fuel Safety Branch,
Chalk River Laboratories, Chalk River, Ontario, Canada

Received February 11, 2000

Accepted for Publication August 16, 2000

KEYWORDS: iodine-assisted corrosion, stainless steel sampling lines, iodine sorption model

Previous experimental work led to the development of a kinetic model that can be used to quantify iodine sorption behavior on a stainless steel surface. The kinetic model, based on the mechanism proposed in earlier work, consists of four chemical reactions. The model has reproduced the time-dependent adsorbed iodine concentration data on the coupons observed under various atmospheric conditions and different cycles of loading and purging. The iodine adsorption kinetics were then incorporated into a mass transport equation to simulate iodine sorption behavior from a flowing air stream through a length of stainless steel tubing. Discussed are the model, the simulation results, and their implications regarding the calibration of iodine transmission through long stainless steel sampling lines used for radiological monitoring of airborne iodine in a reactor containment building following an accident.

I. INTRODUCTION

Iodine is regarded as one of the most hazardous fission products that could be released from fuel in the event of a nuclear reactor accident. Under most accident conditions, the iodine released from fuel into the containment building would be primarily in its reduced state as cesium iodide. In this form, it would be readily dissolved in the water present in containment, discharged from a break in the heat transport system, or released by any safety systems.¹⁻⁴ In the presence of a high radiation field following an accident, however, the dissolved iodide slowly oxidizes to volatile I₂ and organic iodides, and it

can become airborne.^{5,6} If the accident mitigation strategy involves an active intervention, it would be useful to be able to measure the airborne iodine concentration in containment to determine when the intervention would be most opportune.

Radiological monitoring of the airborne iodine concentration in containment following an accident often requires air sampling through long stainless steel lines to minimize background contributions. Quantifying the interaction of iodine with stainless steel is thus very important in any attempt to calibrate iodine transmission through the gas sampling lines. The work presented here was initiated to develop an understanding of the interaction of gaseous I₂ in stainless steel sampling lines. However, the results can be also used to predict iodine behavior in containment following an accident, as stainless steel structures are present in containment. The ability to predict the extent of I₂ interaction with steel surfaces following an accident is desirable.

We previously reported on an experimental study of the iodine adsorption and desorption behavior on stainless steel (Type 304-L) surfaces under ambient temperature and atmospheric conditions.⁷ The study consisted of iodine sorption kinetic measurements and surface analyses. The sorption kinetics were studied by measuring the ¹³¹I activity on stainless steel coupons as a function of time during loading with I₂, labeled with ¹³¹I, and during purging. Loading was conducted by deposition from a flow of N₂ or air until saturation or a steady state was reached. This was followed by purging with N₂ or air until no iodine desorption was observed. Inactive experiments were also done so that scanning electron microscopy (SEM) photographs and energy disperse X-ray spectroscopy analyses could be obtained at various stages of loading and purging. These experiments were performed on various stainless steel surfaces (untreated, electropolished, and nitric-acid treated) and for multiple (up to four) cycles of loading and purging. Based on these results, possible mechanisms for the interaction of iodine

*E-mail: wrenc@aecl.ca

with stainless steel were proposed. This work led to the development of a kinetic model that can be used to quantify iodine sorption behavior on stainless steel.

This paper describes the model and presents model simulation results for the iodine sorption tests previously reported.⁷ The sorption model is then incorporated into a mass transport equation to characterize iodine behavior in gas flowing through stainless steel tubing, and to assess implications regarding the calibration of iodine transmission from long stainless steel sampling lines used for radiological monitoring of airborne iodine in a reactor containment building following an accident.

II. DESCRIPTION OF THE KINETIC MODEL

The kinetic model developed to quantify iodine sorption on stainless steel at ambient temperature and low relative humidity (<35%) consists of four reactions shown in Table I. The gas phase iodine-accelerated corrosion of stainless steel is a complex process to model. It is unlike uniform monolayer adsorption, which is readily described in physical terms. The iodine sorption and subsequent stainless steel corrosion is highly localized and progresses very rapidly, forming highly defected crystals or solids (these solids grow to be ~1 μm deep and

100 μm in diameter). Furthermore, stainless steel is a complex alloy, and its surface (especially that of untreated material) is not easy to characterize or to prepare consistently. Considering the complexity of the realistic system that was studied, the description of the process using only four reactions may be too simplistic an approach to represent all the physical processes in detail. What is attempted in the present studies is to develop a practical model that

1. Is based on a mechanistic understanding so that the model is robust, i.e., can be used with some confidence over a broader range of conditions than those studied.

2. Can be used as an analysis tool to extract fundamental parameters for iodine uptake on stainless steel from which a coherent database can be constructed. For example, surface sorption kinetics are often described and reported using only a single deposition velocity. It will become clear in Secs. IV and V that the deposition velocity is neither an adequate nor sufficient parameter for describing the kinetics of iodine uptake on stainless steel surfaces.

The kinetic model to simulate the iodine adsorption and desorption on a stainless steel surface and its accompanying corrosion is based on experimental studies

TABLE I
Reactions in the Iodine Sorption Kinetic Model

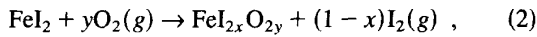
Reaction Number	Reaction	Rate ^a
R1	$\text{Fe}(b) + \text{I}_2(g) \rightarrow \text{FeI}_2$	$k_{AD} \cdot \left(1 - \frac{[\text{Scale}]_t}{[\text{Fe}(b)]_0}\right) \cdot [\text{Fe}(b)] \cdot [\text{I}_2(g)]$ $k_{AD} = 5 \times 10^5 \text{ cm}^3 \cdot \text{mol}^{-1} \cdot \text{s}^{-1}$
R2a	$\text{FeI}_2 + \text{O}_2(g) \rightarrow \text{FeO}_x + \text{I}_2(g) + (1 - x/2) \text{O}_2(g)$	$k_{2a} \cdot \left(1 - \frac{[\text{Scale}]_t}{[\text{Fe}(b)]_0}\right) \cdot [\text{FeI}_2] \cdot [\text{O}_2(g)]^b$ $k_{2a} = 0.195 \text{ cm}^3 \cdot \text{mol}^{-1} \cdot \text{s}^{-1}$
R2b	$\text{FeI}_2 + \text{O}_2(g) \rightarrow \text{Fixed-I}_2$	$\left(A + B \cdot \left(\frac{[\text{Scale}]_t}{[\text{Fe}(b)]_0}\right)\right) \cdot [\text{FeI}_2] \cdot [\text{O}_2(g)]$ $A = 0.08 \text{ cm}^3 \cdot \text{mol}^{-1} \cdot \text{s}^{-1}$ $B = 0.25 \text{ cm}^3 \cdot \text{mol}^{-1} \cdot \text{s}^{-1}$
R3	$\text{Imp} + \text{I}_2(g) \rightarrow \text{FeI}_2$	$k_{imp} \cdot [\text{Imp}] \cdot [\text{I}_2(g)]^c$ $k_{imp} = 6 \times 10^7 \text{ cm}^3 \cdot \text{mol}^{-1} \cdot \text{s}^{-1}$

^a $[\text{Fe}(b)]$, $[\text{FeI}_2]$, $[\text{Imp}]$, $[\text{FeO}_x]$, and $[\text{Fixed-I}_2]$ are in units of mole per square centimetre, whereas $[\text{O}_2(g)]$ and $[\text{I}_2(g)]$ are in units of mole per cubic centimetre.

^b $[\text{Scale}]_t$ is the surface concentration of oxy-iodides scale at time t and is defined in the model as follows: $[\text{Scale}]_t = [\text{FeI}_2]_t + [\text{FeO}_x]_t + [\text{Fixed-I}_2]_t$.

^c $[\text{Imp}]$ is the concentration of impurity on the coupon surface.

reported in Ref. 7. This early study proposed that the following reactions occur on stainless steel surfaces exposed to I₂ in air at room temperature and low relative humidity (<35%):



where Fe(*s*) represents any reactive metal species on the surface (which is likely to be mainly iron and hence the notation Fe; presumably Fe in an oxidation state less than +2 and is referred to as reactive surface Fe hereafter).⁷ The iron oxy-iodides, FeI_{2x}O_{2y}, represents not one compound, but a mixture of iodides, oxy-iodides, and oxides of iron; FeIO, FeO, and Fe₂O₃.

The extent of iodine uptake and corrosion on stainless steel in contact with the gas phase at room temperature is significant, and it appears that iodine adsorbs as easily on corroded surfaces as on a fresh untreated surface. This extensive corrosion in the gas phase was surprising, considering that no electrolytes were present. To account for the ample supply of reactive surface Fe, it was postulated that either (a) the volume changes associated with the formation of FeI₂ and the subsequent FeI_{2x}O_{2y} scale creates cracks that facilitate I₂ diffusion to react with nascent reactive Fe underneath the scale to form FeI₂, (as shown schematically in Fig. 15 in Ref. 7), or (b) the fast iodine-iron interaction forms a highly defective, semiconductor scale, which allows the migration of reactive iron to the surface.

The rate at which reactive Fe becomes exposed to the surface to react with I₂ is modeled using the following first-order process:

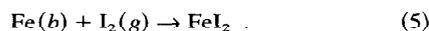


with an overall rate constant, *k*_{Fe(*b*)}. The rate law for reaction (3) is then

$$-\frac{d[\text{Fe}(b)]_t}{dt} = \frac{d[\text{Fe}(s)]_t}{dt} = k_{\text{Fe}(b)} \cdot [\text{Fe}(b)]_t \quad (4)$$

where Fe(*b*) represents the total available amount of base metal that could be exposed to the surface to react with iodine [or become reactive surface Fe, Fe(*s*)], as the reaction progresses. Also, [Fe(*b*)]_{*t*} and [Fe(*s*)]_{*t*} are the concentrations of Fe(*b*) and Fe(*s*) per unit area at time *t* (mol·cm⁻²).

Reaction (1) is fast compared to Reaction (3); thus, Reaction (3) is the rate-determining step for the formation of FeI₂, and the concentration of Fe(*s*) reaches a steady-state at a relatively low level. Thus, for the purpose of kinetic analysis for FeI₂ formation, Reactions (1) and (3) can be combined into one reaction:



The rate of Reaction (5) (or R1 in Table I) is assumed to be proportional to the total available reactive iron concentration, [Fe(*b*)]_{*t*}, and the gas phase iodine concentration, [I₂(*g*)]_{*t*}, but also assumed to slowly decrease as the iron oxy-iodides scale builds up, i.e.,

$$\text{Rate of Reaction (5)} = k' \cdot [\text{Fe}(b)]_t \cdot [\text{I}_2(g)]_t \quad (6)$$

$$k' = k_{AD} \cdot \left(1 - \frac{[\text{Scale}]_t}{[\text{Fe}(b)]_0} \right) \quad (7)$$

$$[\text{Scale}]_t = [\text{FeI}_2]_t + [\text{FeI}_{2x}\text{O}_{2y}]_t \quad (8)$$

where [Fe(*b*)]₀ is the initial concentration of Fe(*b*) (or the total available reactive metal in units of mole per square centimetre), [I₂(*g*)]_{*t*} is the gas phase iodine concentration (in moles per cubic centimetre) at time *t*, and [Scale]_{*t*} is the concentration of iron oxy iodides scale at time *t* (in moles per square centimetre).

Combining Reactions (1) and (3) into Reaction (5), where Reaction (3) is the rate-determining step, implicitly assumes that the rate of Reaction (3) depends on the gas-phase iodine concentration. This assumption is considered to be reasonable for either mechanism (a) or (b), because both the propagation of cracks and the migration of charged particles through the highly defective scale⁸ are expected to increase with the iodine concentration. The rate constant *k*_{AD} is set at 5 × 10³ cm³·mol⁻¹·s⁻¹ for the geometry used in the iodine adsorption tests at room temperature and low relative humidity.⁷ The ratio of volume to geometric surface area in the experiments was ten. The value of *k*_{AD} was chosen because it gave the optimum simulation results for all tests (see Sec. III).

During the iodine sorption tests on coupons,⁷ the gas-phase iodine concentration was constant with time during iodine loading. For a constant iodine concentration, i.e., [I₂(*g*)]_{*t*} = [I₂(*g*)]₀, the rate Eq. (6) for Reaction (5) (or R1 in Table I) would result in a near exponential decrease of the rate:

$$[\text{Fe}(b)]_t \approx [\text{Fe}(b)]_0 \cdot \exp(-k' \cdot [\text{I}_2(g)]_0 \cdot t) \quad (9)$$

The term “near exponential” is used because the dependence of the rate constant on the scale buildup [see Eq. (7)] was ignored while obtaining this analytical solution. The decrease in the bulk Fe(*b*) concentration with time is, in physical terms, equivalent to the decrease in the available surface area of Fe(*b*) to be exposed to I₂ as the scale forms. The oxide scale formation observed during the iodine-catalyzed corrosion of stainless steel⁷ appears to be similar to the scale formation observed during air-oxidation at high temperatures.⁸ The scale formation at high temperature often shows an exponential dependence on time. Reaction (5), or the corresponding rate Eq. (9), results in a near exponential increase in iron oxy-iodides scale as a function of time because

$$\begin{aligned}
 [\text{Scale}]_t &= [\text{FeI}_{2x}\text{O}_{2y}]_t + [\text{FeI}_2]_t \\
 &\approx [\text{Fe}(b)]_0 - [\text{Fe}(b)]_t \\
 &\approx [\text{Fe}(b)]_0 \cdot (1 - \exp(-k' \cdot [\text{I}_2(g)]_0 \cdot t)) \quad (10)
 \end{aligned}$$

where $[\text{FeI}_2]_t$ and the steady-state $[\text{Fe}(s)]_t$ would be very small. The exponential dependence of $[\text{Fe}(b)]_t$ with time is not only consistent with the qualitative behavior of the observed scale formation during iodine interaction with stainless steel, but also has reproduced the iodine adsorption and desorption data reasonably well as shown in Sec. III.

It is also assumed in the model that the rate constant, $k_{\text{Fe}(b)}$, decreases slowly as the scale builds up, hence the need for the second term in the right side of Eq. (7). This suggests that a diffusion process becomes rate determining at the later stage of the iodine-iron interaction. As the corrosion progresses, it would be more difficult for iodine to diffuse through the cracks or for $\text{Fe}(b)$ to diffuse through the scale to the surface.

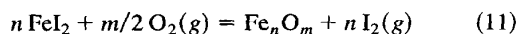
The earlier studies⁷ also suggest that the iodine desorption behavior in the presence of air can be described by Reaction (2). The underlying assumptions of Reaction (2) implicitly state that

1. Adsorbed iodine exists in two species, FeI_2 and $\text{FeI}_{2x}\text{O}_{2y}$.

2. All of the iodine in the form of $\text{FeI}_{2x}\text{O}_{2y}$ is trapped.

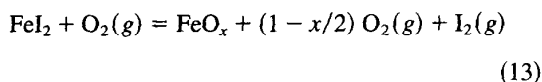
3. In the presence of oxygen in the flow, a fraction of iodine adsorbed as FeI_2 is released (fraction = $1 - x$) and the remaining iodine (fraction = x) forms $\text{FeI}_{2x}\text{O}_{2y}$.

Neither the exact nature of the iron oxy-iodides, nor its exact stoichiometry is known. However, it was observed that the fraction of iodine released changed as the number of loading and purging cycles increased. This suggests that Reaction (2) may proceed through paths, such as

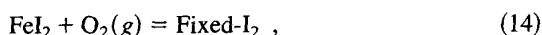


where Fe_nO_m represents a mixture of various iron oxides, and the iron products Fe_nO_m and FeIO together represent the solid oxy-iodides.

In the kinetic scheme, Reaction (2) is modeled using two second-order reactions as follows [Reactions (R2a) and (R2b) in Table I]:



and



where FeO_x and Fixed-I_2 do not represent the formula of real compounds, but together they form iron oxy-iodides,

$\text{FeI}_{2x}\text{O}_{2y}$. Thus, in the model, the scale concentration is defined as

$$\begin{aligned}
 [\text{Scale}] &= [\text{FeI}_2] + [\text{FeI}_{2x}\text{O}_{2y}] \\
 &= [\text{FeI}_2] + [\text{FeO}_x] + [\text{Fixed-I}_2] \quad (15)
 \end{aligned}$$

The second-order rate constants of Reactions 2a and 2b in Table I are defined in the model as

$$k_{R2a} (\text{cm}^3 \cdot \text{mol}^{-1} \cdot \text{s}^{-1}) = 0.195 \times \left(1 - \frac{[\text{Scale}]}{[\text{Fe}(b)]_0}\right) \quad (16)$$

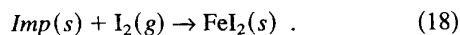
and

$$k_{R2b} (\text{cm}^3 \cdot \text{mol}^{-1} \cdot \text{s}^{-1}) = 0.008 + 0.25 \times \left(\frac{[\text{Scale}]}{[\text{Fe}(b)]_0}\right) \quad (17)$$

such that the branching ratio [or fraction, x , in Reaction (2)] changes with the buildup of iron oxy-iodides scale. The rate constants defined in these equations reproduce the observation that the fraction of adsorbed iodine removed during purging decreased progressively with increasing number of loading and purging cycles. The observation that the fraction, $(1 - x)$, decreases as the number of the cycle increases (i.e., as the corrosion of the surface progresses) can be explained if the increasing $\text{FeI}_{2x}\text{O}_{2y}$ layer could more easily trap the residual iodine in the scale with successive cycles.

Reactions (R2a) and (R2b) and their rates in Table I are represented using a first-order dependence on oxygen concentration for convenience. The actual dependence on oxygen concentration is not known and was not studied. However, for the purpose of this work, the first-order dependence was used to simplify the chemical model. The oxygen concentration in the air flow used in the experiments was $[\text{O}_2(g)] \approx 1 \times 10^{-5} \text{ mol} \cdot \text{cm}^{-3}$.

Impurity sites on the surface (e.g., defect sites inherent on stainless steel surfaces such as sulfur or other trace components, residual metal fragments from cutting tools, or water droplet and contaminants introduced while cleaning and handling) for I_2 to react, have been observed.⁷ These impurities are believed to be responsible for the quick initial adsorption observed. The reaction of the impurities with iodine is modeled as [Reaction (R3) in Table I]:



It is assumed that the iodine reaction with impurities produces metal iodide (represented here as FeI_2), which then subsequently undergoes Reaction (2). The rate constant of Reaction (18), k_{imp} , was set to be $6 \times 10^7 \text{ mol}^{-1} \cdot \text{cm}^3 \cdot \text{s}^{-1}$; however, in the simulations, the impurity concentration was adjusted to give best fits for the loading and purging data for each cycle (see Sec. III). The product, $k_{\text{imp}} \cdot [\text{Imp}]_0$, is thus the meaningful quantity.

TABLE II
Coupon Simulation Parameters

Case Number	Cycle	Atmosphere Loading/Purging	$[I_2(g)]$ (mol·cm ⁻³)	$[Fe(b)]_0$ (mol·cm ⁻²)	$[Imp]_0$ (mol·cm ⁻²)
1	1	N ₂ /N ₂	8.70E-13 ^a	2.2E-7	5E-11
2	1	N ₂ /N ₂ and air	4.10E-12	1.0E-7	0.6E-8
3	1	Air/air	2.21E-12	1.4E-7	0.75E-8
	2		2.52E-12		0.85E-8
	3		1.05E-12		0.4E-8
	4		2.43E-12		1.2E-8
4	1	Air/N ₂	2.13E-12	1.4E-7	0.3E-8
	2		8.30E-13		0.25E-8

^aRead as 8.70×10^{-13} .

The reaction kinetics, consisting of Reactions (R1), (R2), and (R3) in Table I, was solved using the FACSIMILE code,⁹ a commercial integration package for solving coupled-differential equations that was specifically designed for chemical kinetic problems.^a

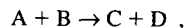
III. MODEL SIMULATIONS OF COUPON TESTS

III.A. Simulated Cases

Four iodine loading and purging cases on untreated stainless steel surfaces reported in Ref. 7 were simulated using the reaction kinetic model shown in Table I:

1. *case 1*: one cycle of I₂ loading in N₂, followed by purging with N₂

^aIn FACSIMILE, the chemical system to be modeled is expressed as a series of simple chemical reactions as an input, which is then converted into coupled differential equations and solved by a numerical integration method. For example, when a chemical reaction



with a rate constant of k is entered, FACSIMILE converts the chemical reaction into a series of coupled differential rate equations:

$$\frac{d[A]}{dt} - \frac{d[B]}{dt} = -k[A][B]$$

and

$$\frac{d[C]}{dt} = \frac{d[D]}{dt} = k[A][B].$$

FACSIMILE then solves the differential equations simultaneously.

2. *case 2*: one cycle of I₂ loading in N₂, followed by a N₂ purge and an air purge
3. *case 3*: four cycles of I₂ loading and purging with air
4. *case 4*: two cycles of I₂ loading in air, followed by purging with N₂.

Each case represents a test or a series of tests performed with the same stainless steel coupon specimen. In each cycle, iodine loading, in general, continued until a steady-state was reached. Subsequent purging also continued until a new steady state was reached. The time intervals between cycles displayed in the figures do not necessarily reflect the true delay between each cycle. Although the specimen was stored under nitrogen between cycles, rigorous attempts to completely avoid contact with oxygen or water vapor were not made. All cases simulated were performed using untreated stainless steel.

The boundary or initial conditions used for each simulation were as follows:

1. $[I_2(g)]_t$ and $[O_2(g)]_t$ were the actual concentrations used in each test and were constant with time, i.e., $[I_2(g)]_t = [I_2(g)]_0$ and $[O_2(g)]_t = [O_2(g)]_0$.
2. The initial concentrations of $[FeI_2]$, $[FeO_x]$ and $[Fixed-I_2]$ were zero.
3. The initial concentration of Fe(*b*), $[Fe(b)]_0$, which is equivalent to the total amount of iron that can migrate to the surface to be available for reaction, was specimen-dependent, i.e., adjusted to give the best fit for a given case.
4. The initial concentration of impurities, $[Imp]_0$, was adjusted to give the best fit for each cycle.

The values of $[I_2(g)]_0$, $[O_2(g)]_0$, $[Imp]_0$, and $[Fe(b)]_0$ used for simulations are listed in Table II.

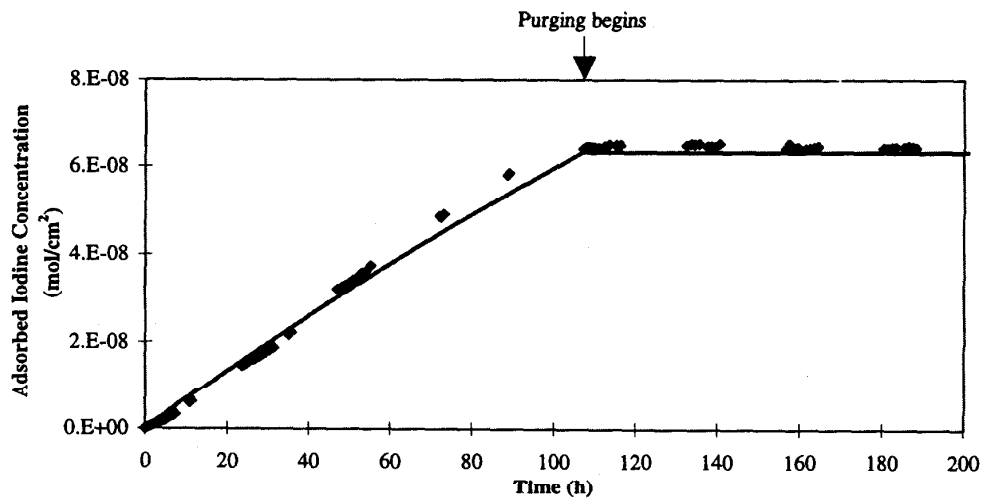


Fig. 1. Adsorbed iodine concentration on an untreated stainless steel coupon during loading and purging in N₂ (case 1); symbols are the experimental data, and the line is the simulation.

For a given set of initial conditions, the model calculated the concentrations of all species as a function of time. The calculated adsorbed iodine concentration, which is the sum of 2 · [FeI₂] and 2 · [Fixed I₂], was then compared with the observed concentration in units of I mol · cm⁻³. Another interesting result is the extent of scale formation. The calculated iron oxy-iodide scale concen-

tration is the total Fe reacted and is the sum of [FeI₂], [FeO_x] and [Fixed-I₂] [Eq. (15)].

III.B. RESULTS AND DISCUSSION

Model simulation results are compared with experimental data in Figs. 1 through 8. Also shown in Figs. 4

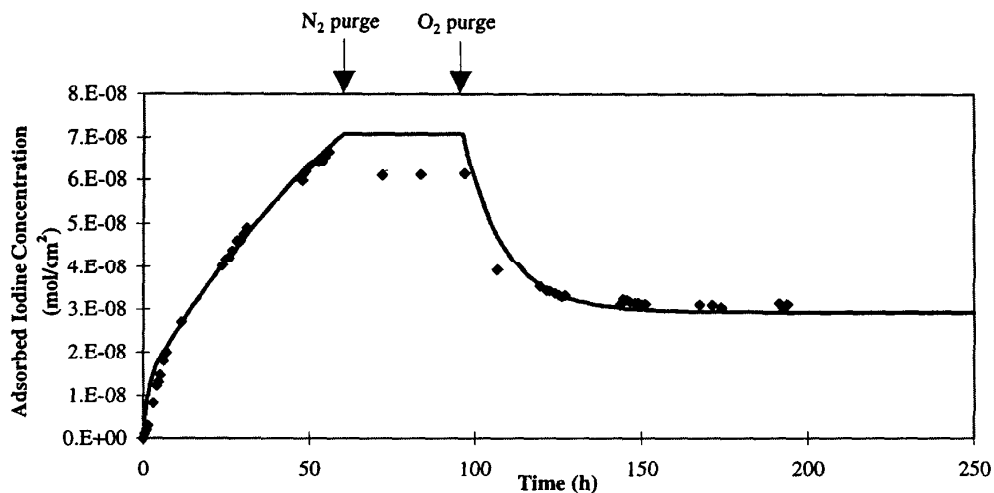


Fig. 2. Calculated concentration of surface species on an untreated stainless steel coupon during loading and purging in N₂, and subsequent purging with air (case 2). Symbols are the experimental data, and the line is the simulation.

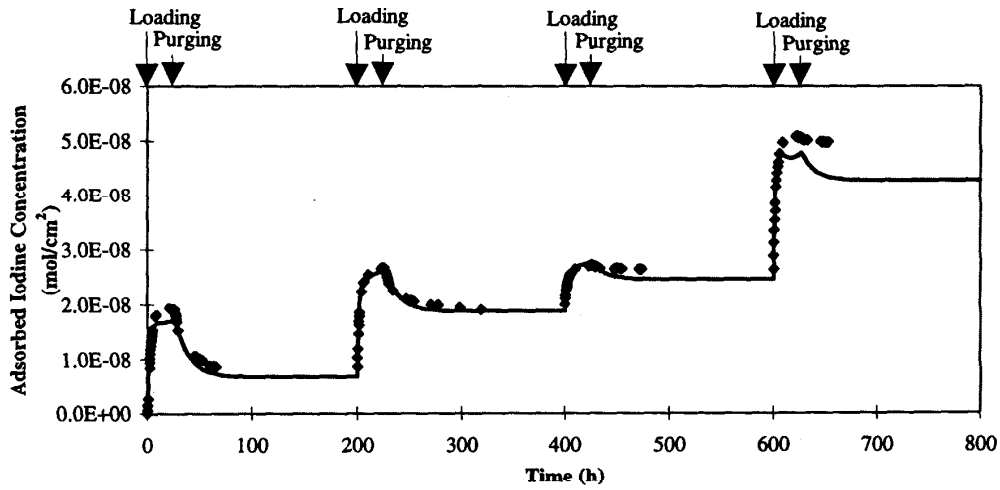


Fig. 3. Adsorbed iodine concentration on an untreated stainless steel coupon during loading and purging in air (case 3). Symbols are the experimental data, and the line is the simulation.

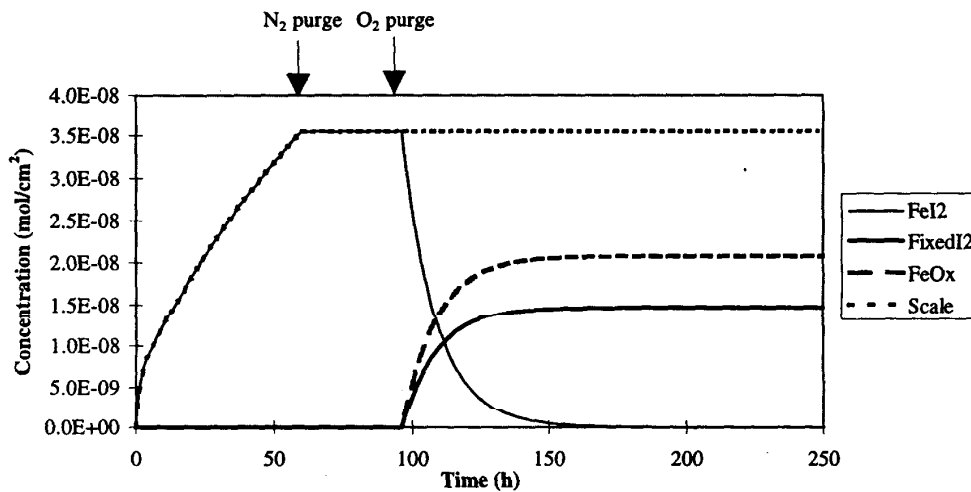


Fig. 4. Calculated concentration of surface species on an untreated stainless steel coupon during loading and purging in N₂, and subsequent purging with air (case 2). Scale is the sum of FeI₂, Fixed-I₂, and FeO_x.

and 5 are the accompanying calculated iron oxy-iodides scale concentrations. The simple model, consisting of four reactions, reproduces the iodine adsorption-desorption behavior observed under various flowing conditions reasonably well, considering that the modeled system is complex and difficult to characterize in detail.

The simplest case is case 1 where the loading and purging take place under a nitrogen environment. Because iodine desorption requires oxygen, there is no de

sorption during the nitrogen purge (Fig. 1). Case 2 reiterates this point by desorbing iodine only during the portion of purging when air is introduced (Fig. 2)

Case 3, loading and purging in air, is shown in Fig. 3. Iodine uptake in air in each cycle is smaller than that in N₂. In air, the adsorbed iodine concentration reaches a steady-state value during loading. It decreases during purging in air, however, reaching another steady-state value.

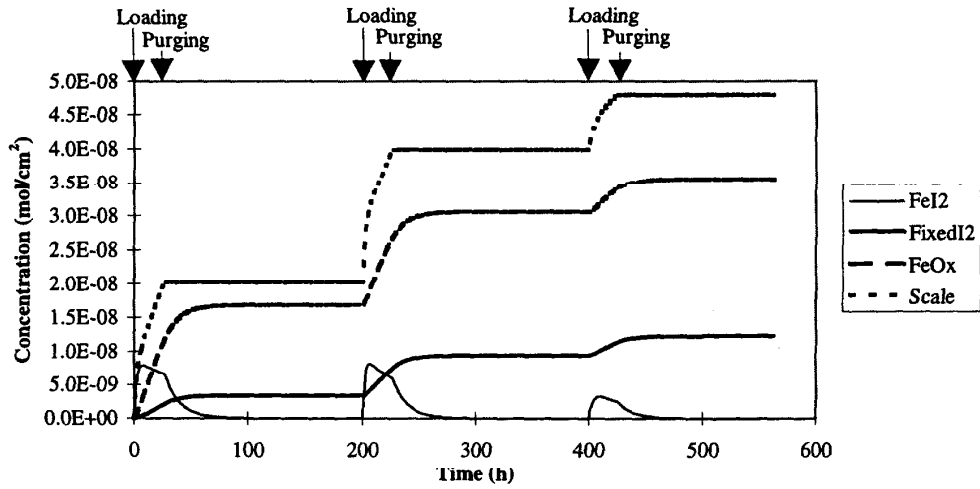


Fig. 5. Calculated concentration of surface species on an untreated stainless steel coupon during loading and purging in air (case 3). Scale is the sum of FeI_2 , Fixed- I_2 , and FeO_x .

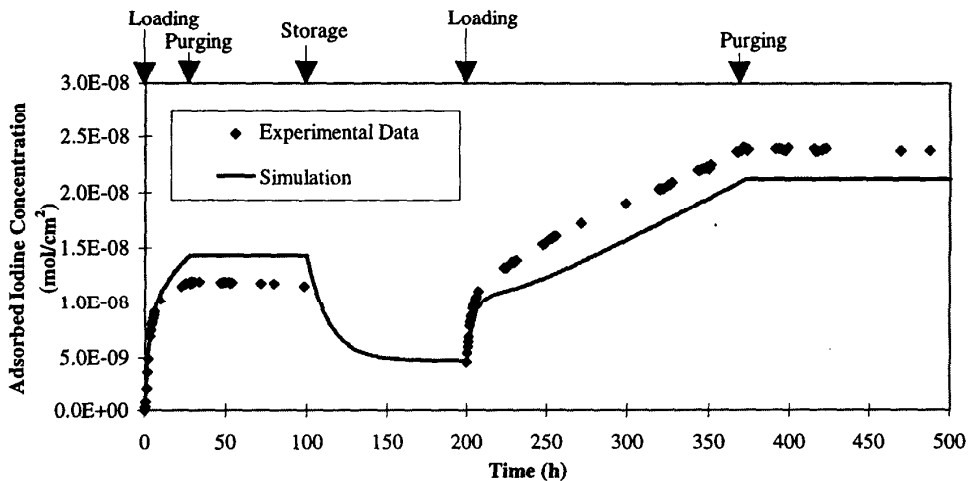


Fig. 6. Adsorbed iodine concentration on an untreated stainless steel coupon during loading in air and purging with nitrogen (case 4). Symbols are the experimental data, and the line is the simulation.

The calculated scale concentrations, shown in Figs. 4 and 5, explain the observations that despite a smaller uptake of iodine, the surface at the end of the test appeared to be more extensively corroded during loading in air than during loading in N_2 (compare SEM photographs shown in Figs. 9, 10, and 11 of Ref. 7). The formation of FeO_x and Fixed- I_2 (or lack of) also explains why the amount of loading in the nitrogen case (case 2) is higher and does not appear to reach a maximum as it does in the air cases

(case 3). Under nitrogen, the product of the reaction (or the scale) is made up entirely of FeI_2 , whereas in air, the scale is a constantly changing mixture of FeI_2 , FeO_x , and Fixed- I_2 . Under air conditions, newly formed FeI_2 is constantly being desorbed and converted to the other scale products, reducing (and even stopping) the overall observed iodine adsorption rate. The consumption of available base metal, $Fe(b)$, is the same in either case, as they are both limited by the diffusion of $Fe(b)$ to the surface

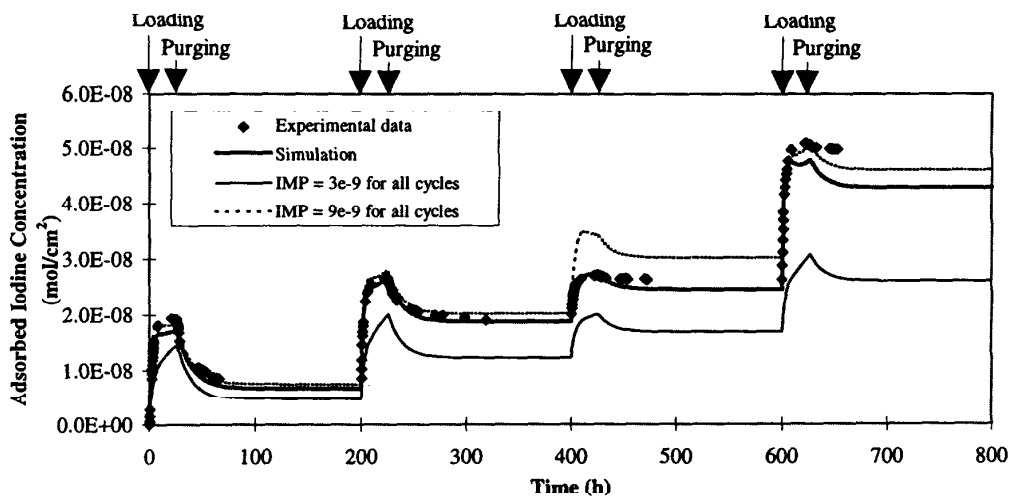


Fig. 7. Adsorbed iodine concentration on an untreated stainless steel coupon during loading and purging in air (case 3). Symbols are the experimental data, and the lines are simulations to demonstrate the range in iodine loading behavior caused by the uncertainty in impurity concentration.

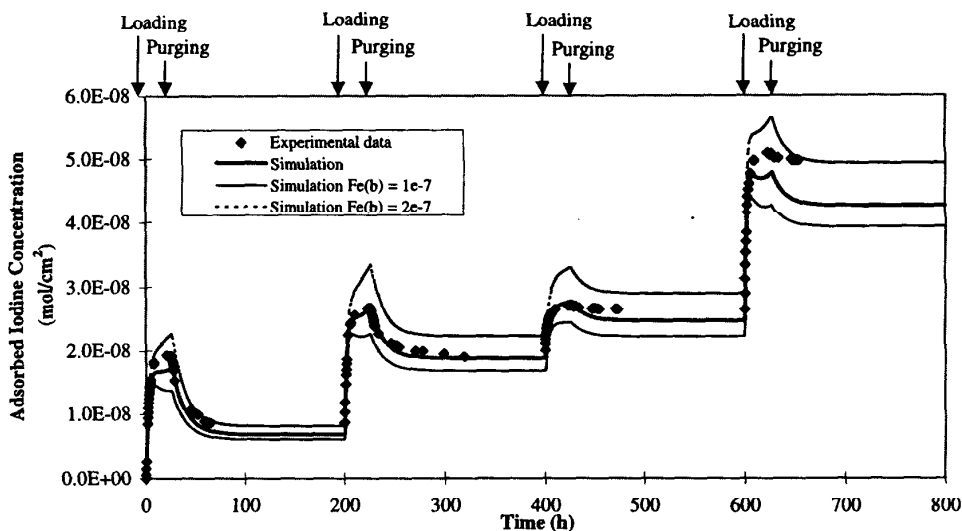


Fig. 8. Adsorbed iodine concentration on an untreated stainless steel coupon during loading and purging in air (case 3). Symbols are the experimental data, and the lines are simulations to demonstrate the range in iodine loading behavior caused by the uncertainty in the bulk phase iron (Fe(b)) concentration.

to react with I₂ [Reaction (R1)]. A significant volume change also appears to accompany the conversion of FeI₂ to FeO_x and Fixed-I₂, which explains the observed increase in localized corrosion under the air environment. The simulation of case 3 (Figs. 3 and 5) displays the progressive buildup of scale on the surface as the number of loading and purging cycles increases.

Case 4 is the case loaded in air and purged with nitrogen (Fig. 6). It is suspected that coupons were exposed to air while being handled following each cycle, and while being stored between the cycles. This might have caused the desorption after the nitrogen purge. Cycle 2 in case 4 in the model calculations was initiated at the point at which a steady state for the adsorbed iodine

concentration was reached assuming air exposure. Case 4 was the worst case in terms of reproducibility, possibly due to the uncertainty associated with oxygen contact during manipulation and storage of the coupons. The model, however, still reproduces the adsorbed iodine concentration to within $\pm 20\%$.

The initial concentration of $Fe(b)$, $[Fe(b)]_0$, required to simulate the data ranged from 1×10^{-7} to 2×10^{-7} mol·cm⁻², and the level of impurities, $[Imp]_0$, ranged from 3×10^{-9} to 2×10^{-8} mol·cm⁻². Note that the stainless steel coupons (12.7 mm in diameter, 3 mm in thickness) were all prepared from Type 304-L stainless steel rods. Each coupon was washed, sequentially, in distilled water, 2-propanol, acetone, and methanol, and then dried at 70°C for 30 min and stored in a desiccator until required. The ranges for $[Fe(b)]_0$ and $[Imp]_0$ obtained from the simulations indicates the degree of surface variation on the samples of Type 304-L stainless steel. The impact of the ranges of these key parameters on the adsorbed iodine concentration is shown in Figs. 7 and 8. In these figures, case 3 is simulated using the minimum and the maximum values of $[Fe(b)]_0$ (Fig. 8) and $[Imp]_0$ (Fig. 7), while the other parameters are held the same as those used for the simulation presented in Fig. 3. These ranges result in a 30% variance in the calculated adsorbed iodine concentrations (per unit area).

IV. APPLICATION OF MODEL TO STEEL SAMPLING LINES

The adsorption kinetic model was also applied to model iodine adsorption from flowing air along the length of stainless steel tubing, using the $[Fe(b)]_0$ and $[Imp]_0$ values determined in the coupon studies. This study was initiated to demonstrate how measurements of iodine adsorption parameters on coupons and tubing are related. The calculations provide an estimate of the magnitude of iodine sorption in sampling lines, although under a very limited set of conditions. The implications of the results are discussed, regarding the calibration of I₂ transmission from long stainless steel sampling lines used for radiological monitoring of airborne iodine in a reactor containment building following an accident.

Note that iodine adsorption was studied at room temperature and low relative humidity, which is not the same conditions expected following an accident. Because the model has been constructed for iodine adsorption at room temperature, the results cannot be extrapolated to the high temperature and relative humidity conditions that could be seen by sampling lines in an accident, without additional support.

Modeling iodine behavior along the length of stainless steel tubing requires solving a one-dimensional convection-diffusion mass transport equation including iodine adsorption and desorption:

$$\frac{d}{dt} C(z, t) = -V_L \frac{d}{dz} C(z, t) + D \frac{d^2}{dz^2} C(z, t) + \frac{A_g}{V_g} \frac{d}{dt} W(z, t), \quad (19)$$

where

$C(z, t)$ = bulk-gas-phase concentration of I₂ at time t and at point z along the length of the tubing (I mol·cm⁻³)

$V_L(t)$ = flow velocity through the tubing (cm·s⁻¹)

D = diffusion coefficient of I₂ in air (or N₂) (cm²·s⁻¹)

$W(z, t)$ = amount of iodine adsorbed at time t and at point z along the length of the tubing (I mol·cm⁻²)

A_g/V_g = ratio of the tubing inner surface area to the gas volume contained by the tubing per length of tubing (cm⁻¹).

The amount of adsorbed iodine, $W(z, t)$, corresponds to $2 \cdot ([FeI_2] + [Fixed-I_2])$ at a given t and z .

Equation (19) is essentially a mass balance equation. The first two terms on the right side of Eq. (19) represent the changes in the iodine concentration in the gas phase as a result of convection and diffusion respectively. The last term represents the change that is due to its adsorption and desorption on stainless steel. Under the forced flow conditions expected in sampling lines, the diffusion term in Eq. (19) can generally be ignored.

To solve the mass balance differential equation, the adsorption term should be defined. The iodine adsorption kinetics presented in Table I defines this term. Thus, by solving the reaction kinetics and the mass transport simultaneously, the adsorbed iodine profile along the tubing can be obtained. The mass balance equation (19), without the diffusion term, was also solved using FACSIMILE, which handles transport using finite element analysis. The tube was divided into eight elements along the length.

To demonstrate the application of the model to the tubing geometry, a 100-cm length of stainless steel tubing with an interior diameter of 0.46 cm ($\frac{1}{4}$ -in. tubing) was chosen. The results are shown in Figs. 9 through 13. The values of the flow velocity V_L , the inlet iodine concentration $[I_2(g)]_{z=0}$, and the initial concentrations $[Fe(b)]_0$ and $[Imp]_0$ used in the calculations, are listed in Table III.

One of the adsorption profiles at various points along the tube at various times is shown in a three-dimensional figure in Fig. 9 (simulation case D-1 in Table III). This figure clearly shows the time-dependent behavior of iodine adsorption monitored at one point on the tube would be very different from that observed in a different point on the tube (Fig. 9). Thus, one cannot extract the

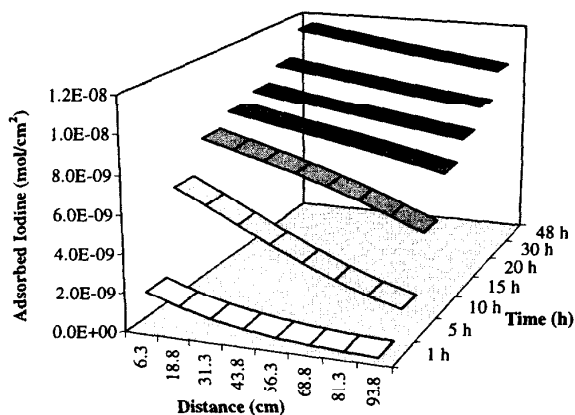


Fig. 9. Adsorption profiles at various points on the tube at various times (Simulation D-1). These were calculated using FACSIMILE, which solves the mass transport using finite element analysis. The number in the distance axis represents the distance from the inlet to the center of each element.

adsorption parameters without considering the mass transport of iodine through the tube, as suggested by Evans et al.¹⁰ and Nugraha¹¹ (see further discussion in Secs. IV and V). This is because adsorption along the tube is not uniform. The adsorption rate in one area is dependent on the gas phase iodine concentration of the upstream zone, and thus is dependent on z .

Even when the mass transport has been properly taken into account, the effects of various parameters on the adsorption profile of iodine on stainless steel tubing are complicated. This point is further illustrated in Figs. 10, 11, and 12, which show the calculated effect of flow rate, inlet iodine concentration, impurity level on the surface, and surface variation on normalized iodine adsorption at

a particular point on the tube. The results in these figures are given in terms of

1. percentage transmission at the outlet of the tube (i.e., percentage of the inlet iodine concentration), which is of interest to sampling line applications for monitoring airborne iodine in containment following an accident
2. the normalized adsorbed iodine concentration as a function of time.

IV.A. Effect of Flow Velocity

The effect of flow velocity on the iodine sorption behavior on stainless steel tubing is shown in Fig. 10 (simulation cases A-1, D-1, and E-1 in Table III). For the simulation cases shown in the figure, $[I_2(g)]_0$, $[Fe(b)]_0$, and $[Imp]_0$ were the same, and only the flow velocity was varied from case to case. In Fig. 10, total gas volume is used as the x axis to normalize the curves with respect to the amount of iodine entering the tube in each case. If the iodine sorption is a simple first-order process that can be expressed with a single deposition velocity, the normalized curves (Fig. 10) should be identical. This is not the case, and the normalized curves show the flow velocity dependence because of the complex iodine uptake behavior on stainless steel. However, the deviation from the linear dependence on flow velocity is less significant than that of inlet iodine concentration.

IV.B. Effect of Inlet Iodine Concentration

This is probably the most important effect for the sampling line applications for monitoring iodine concentration in containment, because the inlet concentration corresponds to the iodine concentration in containment that the radiation monitor at the end of the sampling lines needs to determine. The effect of inlet iodine concentration on the iodine sorption behavior on stainless steel

TABLE III
Tube Simulation Parameters*

Simulation Number	V_z (cm·s ⁻¹)	$[I_2(g)]_{c=0}$ (mol·cm ⁻³)	$[Fe(b)]_0$ (mol·cm ⁻²)	$[Imp]_0$ (mol·cm ⁻²)
A-1	100	2E-12 ^a	1E-7	3E-9
B-1	100	2E-13	1E-7	3E-9
C-1	100	2E-11	1E-7	3E-9
D-1	50	2E-12	1E-7	3E-9
D-2	50	2E-12	2E-7	9E-9
E-1	20	2E-12	1E-7	3E-9
F-1	100	2E-12	1E-7	3E-9, but with one element at 3E-8

*Not all simulation results are shown in the figures or discussed in the text.
^aRead as 2×10^{-12} .

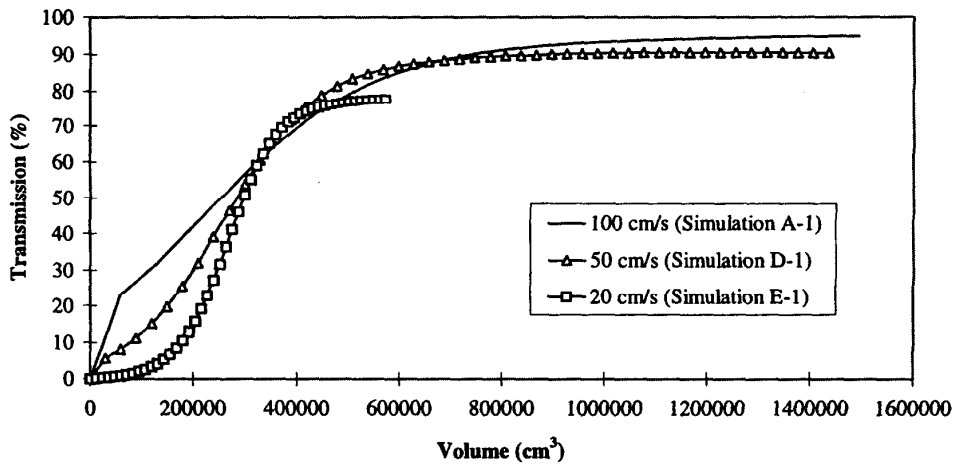


Fig. 10a. Calculated effect of linear flow velocity on simulated transmission through stainless steel tubing. The x axis (volume) is used to normalize the curves with respect to the amount of iodine entering the tube in each case.

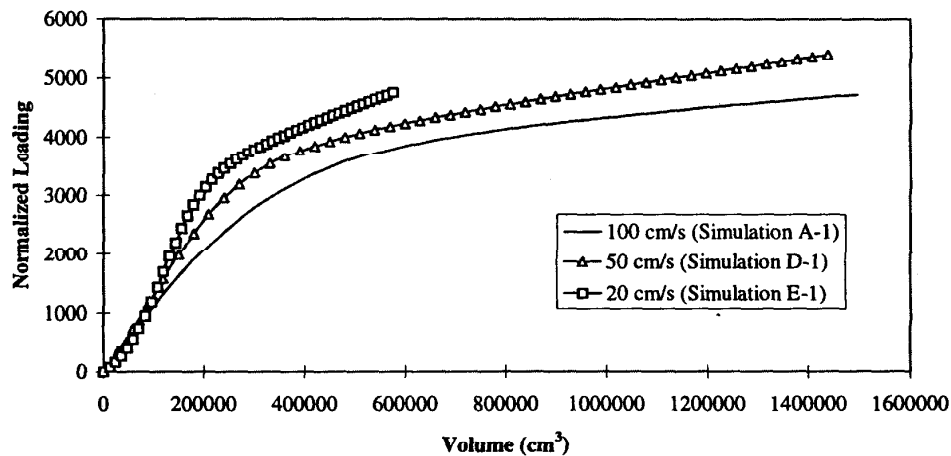


Fig. 10b. Calculated effect of linear flow velocity on iodine adsorption (at 43.75 cm) in a stainless steel tube. The x axis (volume) is used to normalize the curves with respect to the amount of iodine entering the tube in each case.

tubing is shown in Fig. 11 (simulation cases A-1, B-1, and C-1 in Table III, see discussion later for F-1). The iodine transmission and the adsorbed iodine concentration were normalized with respect to the inlet iodine concentration in the figure. For the simulation cases shown in the figure, $[Fe(b)]_0$, $[Imp]_0$, and V_L were the same and only $[I_2(g)]_0$ was varied from case to case.

As with the dependence on flow velocity, if the iodine sorption is a simple first-order process that can be expressed with a single deposition velocity, the normalized curves should be identical. The normalized curves show the inlet iodine concentration dependence because

of the complex iodine uptake behavior on stainless steel. This illustrates that even under the same flow and surface conditions, the percentage transmission strongly depends on the inlet concentration, and that the calibration of iodine transmission through sampling lines would be complicated. Note that the outlet iodine concentration can temporarily exceed the inlet concentration in certain cases when the desorption rate within the tube exceeds the adsorption rate (simulation B-1 in Fig. 11a).

Figure 11b further illustrates the inadequacy of using a single deposition velocity to describe iodine sorption behavior on stainless steel. If one monitors iodine uptake

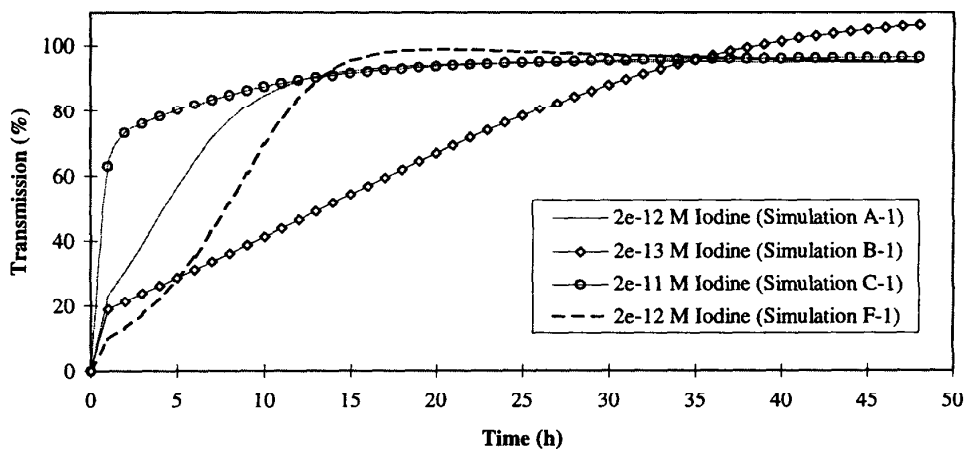


Fig. 11a. Calculated effect of inlet iodine concentration on simulated transmission through stainless steel tubing.

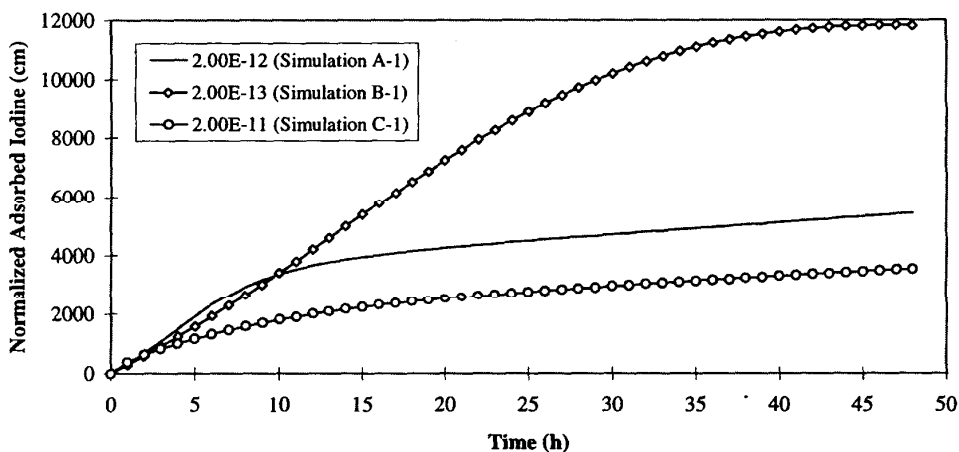


Fig. 11b. Calculated effect of inlet iodine concentration on iodine adsorption (at 93.75 cm) in a stainless steel tube. Adsorbed iodine has been normalized to inlet iodine concentration [adsorbed iodine concentration (mol/cm²) divided by inlet concentration (mol/cm³)].

at a certain point on the tube, one would obtain a different deposition velocity depending on the inlet iodine concentration, which might be interpreted as having a different adsorption mechanism depending on the inlet concentration (see further discussion in Secs. IV and V). Note that all the simulation cases for the tubing geometry use the same adsorption mechanism given in Table I.

IV.C. Effect of Impurity Level and Surface Variation

This effect is also important for the sampling line applications for monitoring iodine concentration in containment, because it determines the uncertainty in the

calibration of iodine transmission, arising from the variation in surface inherent to untreated stainless steel. Figure 12 shows the calculated differences in iodine transmission for the same inlet iodine concentration and flow velocity conditions but for different stainless steel surfaces, i.e., for different $[Fe(b)]_0$ and $[Imp]_0$ (simulation cases D-1 and D-2 in Table III). The ranges of $[Fe(b)]_0$ and $[Imp]_0$ used for the simulations presented in the figure are within their ranges obtained from the simulation of coupon studies, and they correspond to the degree of surface variation on the samples of Type 304-L stainless steel (Sec. III.B). Comparison of Figs. 11 and 12 indicates that the difference in the transmission

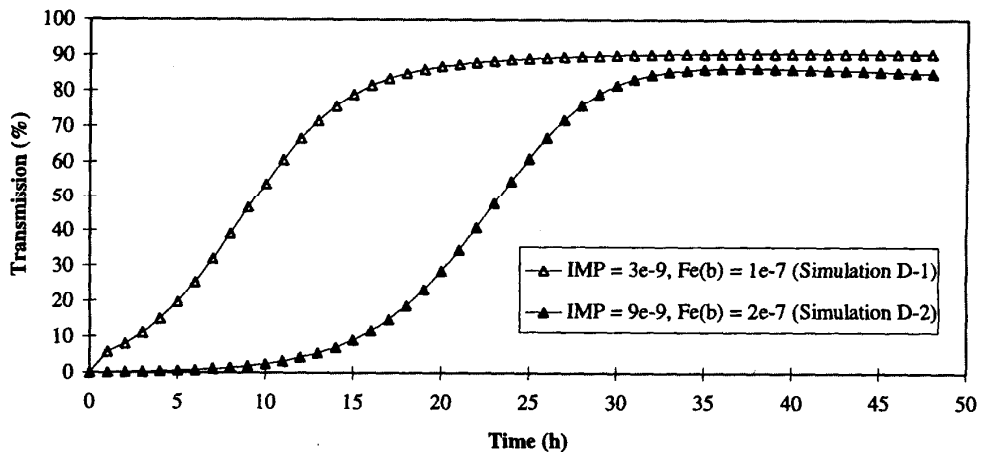


Fig. 12. Calculated effect of impurities and surface iron concentration on simulated transmission through stainless steel tubing.

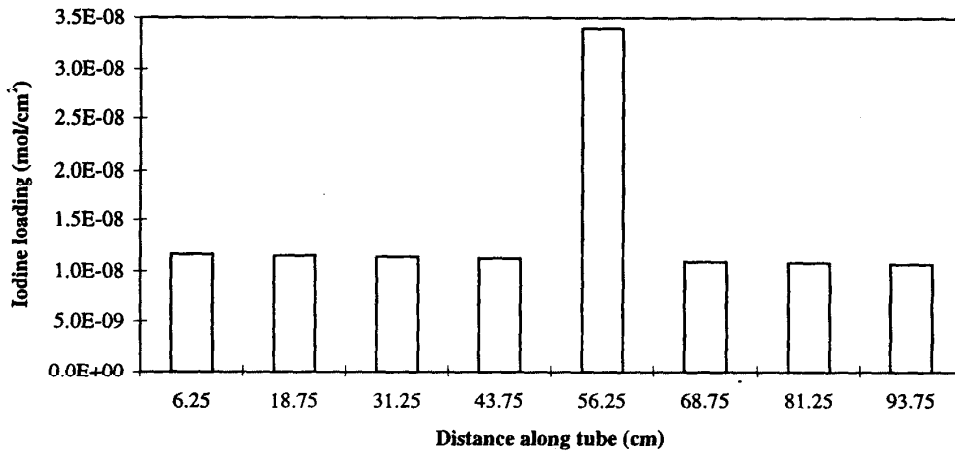


Fig. 13. Calculated iodine loading in a tube that has a higher impurity concentration in the fifth element (simulation F-1, 48 h of loading).

due to stainless steel surface variation would be far greater than the difference in the transmission due to more than an order of magnitude difference in the inlet iodine concentration.

The impact of impurity on iodine transmission is further illustrated by simulation case F-1 in Figs. 11a and 13. The only difference between simulation cases A-1 and F-1 shown in the figure was the impurity level (Table III). The impurity level for A-1 was set to be $3 \times 10^{-9} \text{ mol} \cdot \text{cm}^{-2}$. The impurity level for F-1 was the same as A-1 for most of the elements, except the fifth element (50 to 62.5 cm from the inlet), where the impurity level was set to be $3 \times 10^{-8} \text{ mol} \cdot \text{cm}^{-2}$. Thus, if

a portion of the tube has a high concentration of impurities, adsorption scans with peaks such as those reported by Lee and Jester¹² are possible. Figure 13 shows that a spuriously high adsorption can occur at a position where higher levels of impurities are present on the tubing. This will also decrease the transmission of iodine through the tube (Fig. 11a).

IV.D. Implications for Iodine Sampling Line Calibration

Iodine is easily adsorbed on stainless steel. Depending on the conditions, achieving 100% transmission through a long stainless steel tube may take too long to

be useful (see Figs. 11a and 12). It may be possible to calculate the inlet iodine concentration if the transmission can be calibrated. However, the simulations shown earlier indicate that it may not be feasible considering the effect that uncertainty in bulk iron ($Fe(b)$) and impurity concentration has on transmission (see Fig. 12). The uncertainty in the transmission due to a typical surface variation of untreated stainless steel would be too large to allow for an adequate estimate of iodine transmission through a long tube of untreated stainless steel surface.

Iodine sorption on a stainless steel surface is known to be reduced by various surface treatments such as electropolishing or acid treatment.⁷ These surface treatments, heat treatment, removal of organic impurities, and high flow velocity to minimized time in the line have been suggested to improve iodine transmission and thus to avoid the problems associated with the calibration of the line.¹²

Note that care must be taken when applying the results presented here to sampling in an accident where the temperature and relative humidity are high. It is possible that iodine adsorption mechanisms at a high humidity and a high temperature may be very different from that observed at room temperature and a low relative humidity. In addition, a large fraction of gaseous iodine species in containment following an accident would be organic iodides such as CH_3I (Refs. 5 and 6). Organic iodides are in general less reactive with surfaces as Lee and Jester¹² have shown that CH_3I does not deposit on stainless steel.

V. COMPARISON WITH OTHER WORK

The model presented in this work incorporates mechanisms for both the oxidation of stainless steel surfaces and the desorption of iodine, coupled with a physical model for the transport of iodine. The model is consistent with the experimental findings of many other groups and addresses previously unexplained phenomena.

Previous analyses of iodine adsorption on surfaces often describe adsorption using a deposition velocity, v_d ($cm \cdot s^{-1}$):



$$-\frac{d[I_2(g)]}{dt} = \frac{A}{V} \cdot \frac{d[I(ad)]}{dt} = k \cdot [I_2(g)] \\ = v_d \cdot \frac{A}{V} \cdot [I_2(g)] \quad (21)$$

where k (s^{-1}) = $v_d \cdot (A/V)$ (Refs. 10 and 11). However, our model and the simulation results have shown that because of the interconversion between the species, and the accompanying desorption of iodine, a simple deposition velocity may be neither an appropriate nor a sufficient

parameter to describe iodine adsorption on stainless steel surfaces. The use of deposition velocities is more suited to processes that are known to involve only one step.

The large differences in the deposition velocity as a function of distance from the inlet of stainless steel tubes as observed by Lee and Jester¹² suggests that the use of a simple deposition velocity is inadequate for use in sampling lines under those conditions. The present model is consistent with Lee's findings that transmission of iodine in sampling lines was dependent on sampling flow rate (see Fig. 10a) and the presence of surface contaminants (see Figs. 11a and 12).

The inadequacy of using a simple deposition velocity, without accounting for iodine transport, is also demonstrated by the findings of Evans et al.¹⁰ and Nugraha,¹¹ who, using a deposition velocity model without considering iodine transport through the tube, were unable to explain why iodine adsorption on stainless steel appeared to be very different at low iodine concentrations than at high iodine concentrations. The results can be rationalized by the present model, however, which predicts that the iodine concentration will have a more complex (i.e., nonlinear) impact on the time-dependent adsorption/transmission behavior.

Finally, the simple deposition velocity approach to modeling, even when used in conjunction with corrosion models¹³ cannot account for the iodine desorption behavior observed in experiments reported here and by Rosenberg et al.¹⁴ In agreement with our experiments, Rosenberg reports that deposited iodine appears to be gradually incorporated within corrosion centers on stainless steel, and the extent of corrosion was insignificant in helium, but significant in air. Furthermore, he found that desorption of iodine from stainless steel was enhanced in dry air over that in a steam-air mixture, evidence that the amount of oxygen in the atmosphere controls desorption.

VI. CONCLUSIONS

Several conclusions can be drawn from this study:

1. Iodine adsorption on stainless steel surfaces at room temperature and low relative humidity can be simulated using a very simple model consisting of four reactions listed in Table I.
2. The model accounts for several key observations made during the gaseous iodine sorption experiments on untreated stainless steel coupons reported previously⁷:
 - a. There is higher iodine loading on the surface in the absence of oxygen, compared to in the presence of oxygen.
 - b. There is more significant surface deterioration under oxygenated conditions.

- c. Iodine does not desorb under nitrogen purge and only partially desorbs during an air purge.
 - d. The fraction of iodine remaining in the surface increases upon repeated adsorption/desorption cycles.
3. The values for two of the model parameters, the impurity level on the surface, $[Imp]_0$, and the concentration of total reactive metal, $[Fe(b)]_0$, were surface specific and were not available. Thus, for the simulation of the coupon studies, they were adjusted to give best fits. The ranges of these parameters, obtained from the simulations of the coupon studies, from 1×10^{-7} to 2×10^{-7} mol·cm⁻² for $[Fe(b)]_0$ and from 3×10^{-9} to 2×10^{-8} mol·cm⁻² for $[Imp]_0$, are considered to be the degree of surface variation expected in untreated stainless steel. For a given iodine concentration in the flow (constant with time), these ranges result in a 30% variance in the calculated adsorbed iodine concentrations (per unit area) at room temperature and a low relative humidity.
4. The same iodine adsorption model was then applied to simulate iodine migration through stainless steel tubing. The simulation results illustrate the following:
- a. the difficulties in quantifying iodine adsorption for the purpose of calibrating transmission
 - b. the problems with using tubing experiments to extract adsorption parameters, without consideration of mass transport
 - c. the inadequacy of using a simple deposition velocity in describing iodine sorption on stainless steel.
5. Although they result in a small variance in the adsorbed iodine concentration per unit area, the ranges of the key adsorption parameters [i.e., bulk iron (Fe(b)) and impurity concentrations] are too large to allow for an adequate estimate of the iodine transmission through a long tube of untreated stainless steel, even when temperature and a relative humidity are controlled. Surface preparation, consistency in the surface along the tubing, and exclusion of impurities are therefore very important.

ACKNOWLEDGMENTS

The authors would like to thank J. McFarlane at Atomic Energy of Canada Limited (AECL) and K. Weaver of Ontario Power Generation for helpful discussion and editorial comments. This work was partially funded by the CANDU Owners Group, Research and Development Program, Working Party 06, Containment Behaviour, under the joint participation of Ontario Power Generation, Hydro Quebec, New Brunswick Power, and AECL.

REFERENCES

1. F. GARISTO, "Thermodynamics of Iodine, Cesium and Tellurium in the Primary Heat Transport System Under Accident Conditions," AECL-7782, Atomic Energy of Canada Limited Report, (1982).
2. D. J. WREN, "Kinetics of Iodine and Cesium Reactions in the CANDU Reactor Primary Heat Transport System Under Accident Conditions," AECL-7781, Atomic Energy of Canada Limited (1983).
3. D. CUBICCIOTTI and J. E. SANECKI, "Characterization of Deposits on Inside Surfaces of LWR Cladding," *J. Nucl. Mater.*, **78**, 96 (1978).
4. C. V. MCISAAC and D. G. KEEFER, "Reactor Building Source Term Measurements," *ACS Symp. Ser.*, **293**, 168 (1986).
5. J. C. WREN, J. M. BALL, and G. A. GLOWA, "The Chemistry of Iodine in Containment," *Nucl. Technol.*, **129**, 297 (2000).
6. J. C. WREN, J. M. BALL, and G. A. GLOWA, "The Interaction of Iodine with Organic Material in Containment," *Nucl. Technol.*, **125**, 337 (1999).
7. J. C. WREN, G. A. GLOWA, and J. MERRITT, "Corrosion of Stainless Steel by Gaseous I₂," *J. Nucl. Mater.*, **265**, 161 (1999).
8. M. G. FONTANA, *Corrosion Engineering*, 3rd ed., p. 505, McGraw-Hill Book Company, Toronto, Canada (1986).
9. "FACSIMILE 4.0 Users Guide," AEA Technology, Harwell, United Kingdom (1995).
10. G. J. EVANS, C. DEIR, and J. M. BALL, "The Retention of Iodine in Stainless Steel Sample Lines," *Proc. 23rd Nuclear Air Cleaning and Treatment Conf.*, Buffalo, New York, July 25-28, 1999, NUREG/CP-0141, U.S. Nuclear Regulatory Commission (1994).
11. T. NUGRAHA, "Iodine Retention on Stainless Steel Sampling Lines," MS Thesis, University of Toronto, Department of Chemical Engineering (1997).
12. B.-S. LEE and W. A. JESTER, "Gaseous Radioiodine Deposition Losses in Nuclear Reactor Sample Lines," *Nucl. Technol.*, **113**, 221 (1996).
13. Y. TSUKAUE, G. NAKAO, Y. TAKIMOTO, and K. YOSHIDA, "Initiation Behaviour of Pitting in Stainless Steels by Accumulation of Triiodide Ions in Water Droplets," *Corrosion*, **50**, 10, 755 (1994).
14. H. S. ROSENBERG, J. M. GENCO, and D. L. MORRISON, "Fission Product Deposition and Its Enhancement Under Reactor Accident Conditions: Deposition on Containment-System Surfaces," BMI-1865, Battelle Memorial Institute (1969).

Jungsook Clara Wren (BS chemistry, Sogang University, Korea, 1976; PhD physical chemistry, Kansas State University, 1981) is a senior research scientist in the Fuel Safety Branch at the Chalk River Laboratories of Atomic Energy of Canada Limited (AECL). Her background in nuclear safety research includes the reaction kinetics of iodine species in gas and aqueous phases, iodine surface chemistry, and the abatement of iodine and noble gases. Her other research interests include chemical reactions in high-voltage discharges and radiation fields, and inter- and intra-molecular energy transfer of highly excited molecules.

Glenn A. Glowa (BSc University of British Columbia, Canada, 1990; MSc University of Manitoba, Canada, 1995) is a research scientist in the Fuel Safety Branch at the Chalk River Laboratories of AECL. His current field of study involves several aspects of iodine chemistry that have relevance to reactor safety. This includes the formation and degradation of organic iodides, iodine surface interactions, and kinetic modeling.